IEEE Photonics Journal
An IEEE Photonics Society Publication

Open Access

High-Speed Optical-Beam Scanning by an Optical Phased Array Using Electro-Optic Polymer Waveguides

Volume 12, Number 2, April 2020

Yoshikuni Hirano
Yuji Miyamoto
Masato Miura
Yasushi Motoyama
Kenji Machida
Toshiki Yamada
Akira Otomo
Hiroshi Kikuchi

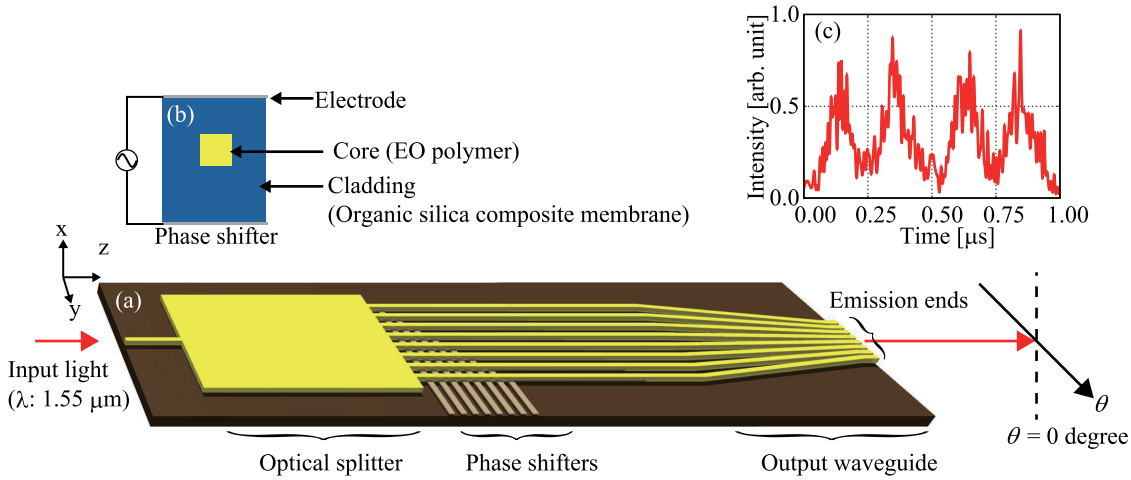

(a) The optical phased array using (b) electro-optic polymer waveguides and (c) variation of light intensity in $\theta = 0$ direction at the siusoidal voltage of 2 MHz applied.

DOI: 10.1109/JPHOT.2020.2981743

High-Speed Optical-Beam Scanning by an Optical Phased Array Using Electro-Optic Polymer Waveguides

Yoshikuni Hirano,[1] **Yuji Miyamoto**,[1] **Masato Miura**,[1] **Yasushi Motoyama**,[1] **Kenji Machida**,[1] **Toshiki Yamada**,[2] **Akira Otomo**,[2] **and Hiroshi Kikuchi**[1]

[1]NHK Science and Technology Research Laboratories, Tokyo 157-8510, Japan
[2]Advanced ICT Research Institute, National Institute of Information and Communications Technology, Hyogo 651-2492, Japan

DOI:10.1109/JPHOT.2020.2981743

Manuscript received February 2, 2020; revised March 9, 2020; accepted March 14, 2020. Date of publication March 18, 2020; date of current version April 13, 2020. Corresponding author: Yoshikuni Hirano (e-mail: hirano.y-cq@nhk.or.jp).

Abstract: Optical phased arrays (OPAs), which manipulate an optical beam by controlling the phase of light, are optical devices characterized by high speed, small size, light weight, and high reliability that make various applications possible. In this study, an eight-channel-waveguide OPA using an electro-optic (EO) polymer for phase control was fabricated. Very high-speed optical beam scanning with a frequency of 2 MHz was demonstrated by applying a driving waveform superimposing sinusoidal and rectangular-wave voltages. Furthermore, the EO polymer OPA can be operated with a low total-operation power consumption of 0.38 mW at a scanning speed of 500 kHz.

Index Terms: Optical phased array, electro-optic polymer, optical waveguides.

1. Introduction

Optical phased arrays (OPAs) enable us to control an individual phase of the divided optical beam to manipulate an interference pattern of a combined optical beam [1]. OPAs have been widely investigated for various applications such as network switches [2], optical interconnects [3], holographic displays [4], and distance-measuring sensors [5]. General OPAs are optical-waveguide devices, and the individual phase of the guided light beam is controlled on the basis of the thermo-optic (TO) and electro-optic (EO) effects, and therefore movable parts (such as polygon mirrors) are unnecessary. Thus, OPAs provide us with beam-manipulation devices with high speed, small size, light weight, and high reliability. OPA-LiDAR (light detection and ranging) has recently attracted much attention in autonomous driving technology. The optical scanning by OPA-LiDAR has been attained by utilizing a large number of arrayed devices [6]. The characteristics of OPA-LiDAR include wide-angle deflection [7], two-dimensional optical-beam scanning [8]–[11], and compatibility with complementary-metal-oxide-semiconductor (CMOS) sensors [3] using silicon optical waveguides suitable for fine and high integration. However, OPAs using a silicon optical waveguide (Si-OPAs) cannot be used in a wavelength less than 1.1 μm due to the absorption loss by silicon. A few studies on optical waveguides for visible light such as silicon nitride waveguides have been reported [12]. Since many Si-OPAs utilize the TO effect as the operation principle for

phase control, issues related to the power consumption and operation speed still remain unsolved. A typical phase shifter utilizing the TO effect changes the refractive index of an optical waveguide with Joule heat generated by a heating electrode located near the silicon waveguide. The typical power consumption required to change the optical phase by a half wavelength is between 10 and 300 mW per channel [10], [13], [14]. Although a high-speed phase shifter with a scanning speed of 350 kHz based on micromechanical systems have been developed [15], the response speed of the phase shifter is restricted due to the operating mechanism. High-speed OPAs using a $LiNbO_3$ (LN) crystal [16], [17], at the steering speed of 40 MHz [18] have been demonstrated; however, the array pitch is large, the scanning angle is small, and the operation voltage is high, which may originate from the difficulty of the microfabrication of LN crystals. The phase control at the modulation frequency of over 1 MHz for OPAs utilizing the EO effect of InP has been suggested [19], [20]; however, the operation of the phase shifter was only confirmed in those literatures. It has been reported that the modulation band of a phase shifter of Si p-i-n phase modulators [21] and GaAs/AlGaAs quantum well phase modulators [22] are 200 MHz and 1 GHz, respectively; however, the power consumption was high due to the carrier injection, and the high-speed beam scanning was not confirmed in those literatures.

EO polymers [23] are significant candidates for OPAs due to their ultra-high-speed response and excellent processability. Since the change in the refractive index of EO polymers is derived from polarizations of π electrons of EO chromophores, EO polymers respond extremely quickly to an external electric field, and phase-control operation at 100 GHz or more have been demonstrated using traveling wave polymer modulators [24]. In addition, EO polymers with a large EO effect has been developed, and their low-power operation can be expected [25]–[28]. We previously demonstrated the basic operation of optical beam scanning via voltage control for OPAs with an EO polymer optical waveguide core for the first time [29]. In this paper, we investigated a driving method for an EO-polymer OPA with organic silica for cladding and the characteristics of the eight-channel-waveguide OPA. Finally, the remarkable performance of the EO-polymer OPA with respect to high-speed optical beam scanning and low-power opration was observed.

2. Device Structure

Fig. 1 shows the structure and operating principle of an EO-polymer OPA. In Fig. 1(a), the light incident on the input optical waveguide is distributed to a multichannel optical waveguide by an optical splitter, and the phases of the guided light beams are individually controlled by the phase shifters. The guided light beams are then emitted from the end face of the output optical waveguides to form an interference pattern. The EO-polymer OPA shown in Fig. 1(a) enables control of the interference pattern in one dimension because the emission ends are arranged linearly in the y-z plane. Distribution $F(\theta)$ of the optical amplitude with respect to angle θ formed with the z-axis of the interference pattern is given by Equation (1), where A_m and φ_m are the amplitude and phase of the m-th outgoing light at a single emission end, k_0 is the wave number of the incident light in vacuum, and p is the pitch of the emission ends.

$$F(\theta) = g(\theta)\Sigma_m A_m \exp(-i\varphi_m) \exp(-ik_0\, mp \sin(\theta)), \tag{1}$$

Here, $g(\theta)$ is the optical amplitude distribution created by a single emission end, and it is known to be a Gaussian distribution. The condition for emitting an optical beam in a specific $\theta = \theta_0$ direction is given as $\varphi_m = k_0\, m\, p \sin(\theta_0)$, and in the case of an EO-polymer OPA, it is controlled using the change in the refractive index of the phase shifter, a cross-sectional view of which is shown in Fig. 1(b). An EO polymer [30] and organic silica are used for the core and cladding material, respectively, and an IZO thin film with a thickness of 100 nm is used for the upper and lower electrodes. The sectional structure of the optical waveguide without the phase shifter is the same as that shown in Fig. 1(b), except that there is no upper electrode. When a core electric field (Ec) is generated by the upper

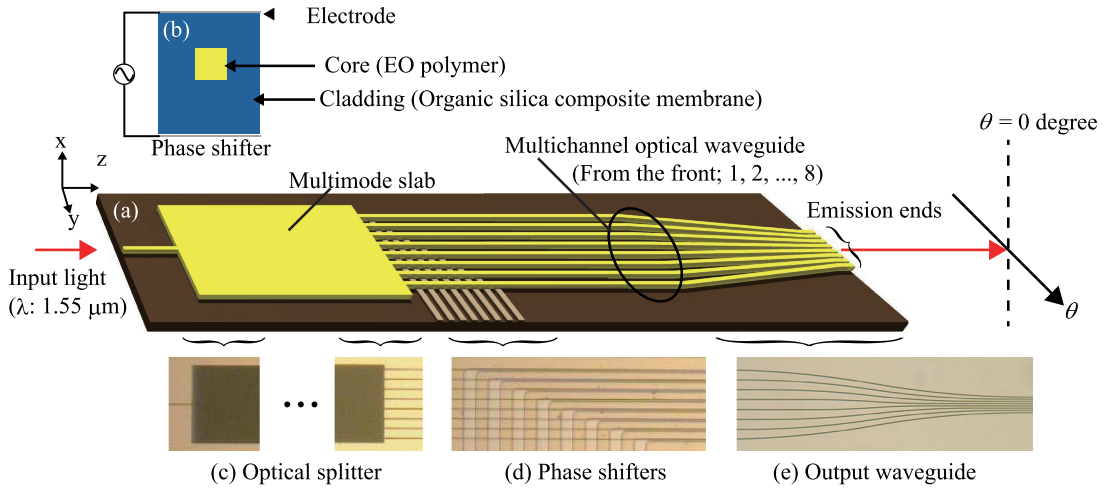

Fig. 1. (a) Outline of the optical phase array (OPA) using EO polymer waveguides fabricated and evaluated in this study. The OPA consists of an 8-waveguide array with a phase shifter and 1 × 8 multi-mode-interference (MMI) optical splitters. (b) Sectional view of the phase shifter that consists of a ridge optical waveguide with a core size of 1.5 μm with 1.5 μm height, an upper-cladding with a thickness of 1.0 μm, a lower-cladding with a thickness of 2.5 μm, and counter electrodes. Microscope images of (c) input and output parts of the 1 × 8 MMI optical splitter, (d) phase shifter, and (e) output waveguide. The width and length of the multimode slab in the MMI optical splitter are 160 μm and 3.3 mm, respectively. The pitch of phase shifters and output channels are 20 μm and 4.5 μm, respectively.

and lower electrodes, the refractive index of the core in the phase shifter $n(Ec)$ is given as

$$n(Ec) = n(0) - \frac{1}{2}n(0)^3 r_{33} Ec, \tag{2}$$

where r_{33} is the EO coefficient.

It has been reported [25], [26] that the use of organic silica for cladding in EO-polymer phase shifters improves the orientation process of EO dyes and improves r_{33}. Furthermore, as the refractive index ($n = 1.48$) of organic silica is smaller than that of a general polymer ($n = 1.6$ to 1.7), the optical confinement of an EO-polymer optical waveguide with organic silica cladding is stronger than that of an all-polymer optical waveguide. The pitch of the multichannel optical waveguide can therefore be narrowed; accordingly, a pitch of 4.5 μm was attained at the emission end.

3. Driving Method and Characteristics

The driving method and characteristics of the EO-polymer OPA are described hereafter. Although an EO polymer is almost insulative at room temperature, it is slightly conductive at high temperatures in the poling process. Accordingly, it is preferable to use a cladding material with a higher conductivity compared with that of EO polymer in order to increase the electric field in EO polymer core in the poling process. The equivalent circuit of a phase shifter at room temperature is composed of upper and lower claddings and side walls (in which a capacitive load and a resistive load are connected in parallel) and a core that is a capacitive load. Thus, it can be modeled by a circuit in which the side wall and the core are connected in parallel, and the upper and lower claddings are connected in series thereto. We consider the frequency characteristics of the model. The voltage subtracted the voltage drop due to the current of cladding from the actual applied voltage is applied to the core at the low-frequency limit, while the voltage corresponding to the capacitance is applied to the core at the high-frequency limit. The half-wave voltage measured in the low-frequency region is not accord with that measured in the high-frequency region. In the middle-frequency region, it is expected that the core voltage for a certain actual applied voltage falls

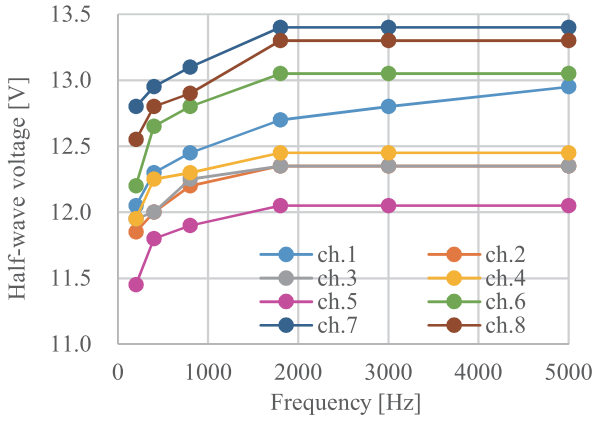

Fig. 2. Half-wave voltage with respect to frequency of a rectangular-wave voltage applied to the phase shifter.

exponentially as the frequency increases, because the charge-discharge cycle of the capacitance is limited by the frequency of a rectangular-wave voltage. Thus, we need to know the frequency dependences of the half-wave voltage in each channel in adjusting the performance of EO-polymer OPA at a certain frequency.

Therefore, the frequency dependence of the half-wave voltage of the fabricated OPA was measured. In the measurement, the half-wave voltage of the phase shifter was determined as the voltage amplitude at which the interference pattern does not vary with time when a rectangular wave voltage is applied. The frequency of the rectangular-wave voltage was set to 400 Hz to 5 kHz in order to avoid a sudden rise in the core voltage in the low-frequency region. The measurement values of the half-wave voltage V_π of the m-th channel ($V_{\pi m}$) with respect to rectangular-wave frequency are shown in Fig. 2. Because the phase shifter capacitance, which depends on width and thickness of the core, varies depending on the deposition and etching processes, the measured values are different for each channel. The core voltage for a certain actual applied voltage increased in the frequency region below 1 kHz, which results in the decrease of $V_{\pi m}$ in the frequency region, while neither the core voltage nor $V_{\pi m}$ vary with frequency when frequency is 2 kHz or more. All eight phase shifters show the same trend. The $V_{\pi m}$ values differ somewhat among eight phase shifters. The phase shifters shown in Fig. 1(b) are fabricated by a fine processing involving various deposition and etching processes. The small differences in the width and thickness of the core and the thicknesses of claddings among the phase shifters may affect the characteristics on $V_{\pi m}$, because the capacitive loads and resistive loads in the equivalent circuit depend on these parameters. Thus, a stable phase control of guided light beam is possible using a modulation frequency of 2 kHz. Therefore, in the subsequent optical beam manipulation experiments, a rectangular wave with a frequency of 3 kHz was used for modulating the phase shifter. The phase of guided light beams was compensated by applying a square-wave voltage of $V_{\pi m}$ to each channel of the phase shifter and then an offset voltage of the m-th channel V_{cm} less than $V_{\pi m}$. Thus, for each channel m, the square-wave voltage $V_{\pi m}$ and offset voltage V_{cm} were applied.

4. Experimental Results

Generally, each V_{cm} is determined by maximizing the optical intensity in the 0-degree direction in Fig. 1. However, as for the end-emission OPA used in this study, sufficient accuracy of V_{cm} cannot be obtained by conventional phase compensation because the stray light caused by coupling and radiation losses is also emitted in the $\theta = 0$-degree direction. Therefore, in addition to conventional phase compensation, optical intensity minimization in the dark-line direction was used. In this compensation method, the optical intensity distribution is normalized using the local maximum

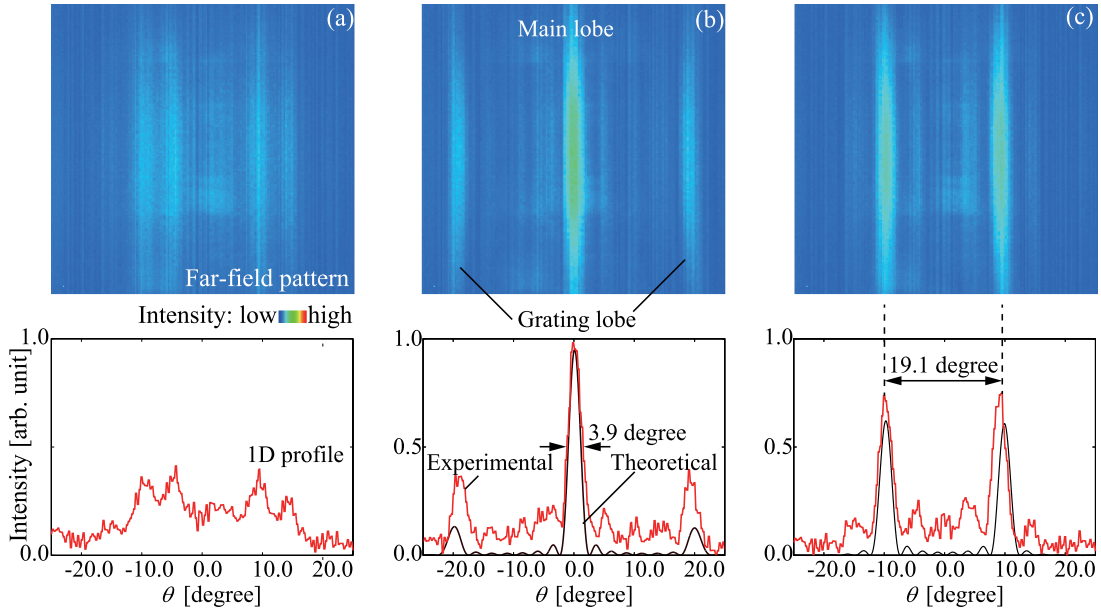

Fig. 3. Far-field patterns and 1D profile of the far-field pattern on the x-y plane (a) without and (b) with phase compensation and (c) with phase compensation by applying $V_{\pi m}$ to the even channels.

intensity between the dark lines. Accordingly, the dynamic range becomes larger than that in the conventional method, because the local maximum intensity is considerably weaker than the main-lobe intensity. For example, when the phase difference between adjacent emitting ends is $\pi/4$, a dark line is formed in the $\theta = 0$-degree direction according to the Equation (1). In this case, the local maximum intensity is about 1/4 times weaker than the main-lobe intensity. Therefore, the phase compensation can be performed with about four times high accuracy, compared with that of the conventional method.

Far-field patterns of an optical beam without and with phase compensation are shown in Figs. 3(a) and (b), respectively. Fig. 3(c) shows the far-field pattern with phase compensation when $V_{\pi m}$ and V_{cm} were applied to the even channels. The theoretically calculated optical intensity distributions are also shown as black lines in Fig. 3(b) and (c). Comparing the experimental ones with the calculated ones, the experimental ones have the background signals which may originate from the stray lights and the influence of the light source spectrum. As shown in Fig. 3(b), the beam divergence angle of the main lobe is 3.9 degrees, which agrees with the theoretical value of 3.8 degrees. As shown in Fig. 3(c), the angle between the main lobe and the grating lobe is 19.1 degrees, which is consistent with the theoretical value. Thus, these results confirm that the designed EO-polymer OPA works accurately.

The characteristics of the EO-polymer OPA with respect to the scanning speed and power consumption were investigated. An experimental system consists of a light source, a polarizer, an EO-polymer OPA, eight function generators, and an InGaAs photodiode. The InGaAs photodiode has a photosensitive area of 0.3 mm^2, which corresponds to approximately a receiving angle of 1.5 degrees. Since the refractive index of the EO polymer core changes in the direction perpendicular to the substrate, incident light in TM mode was input into the EO-polymer OPA. A sinusoidal voltage superimposed on phase-compensation voltage V_{cm} was applied to each channel. Amplitude of the sinusoidal voltage was determined by $V_{\pi m}$ applied to each channel; it was set to 3.5 $V_{\pi m}$, 2.5 $V_{\pi m}$, 1.5 $V_{\pi m}$, and 0.5 $V_{\pi m}$ for channels 1 and 8, 2 and 7, 3 and 6, 4 and 5, respectively. For example, when the scanning frequency is f, the time t dependency of the applied voltage for channel 1 is given by 3.5 $V_{\pi 1}$ $\sin(2\pi ft)$ + V_{c1}. The sinusoidal voltages for channels 1 to 4 and

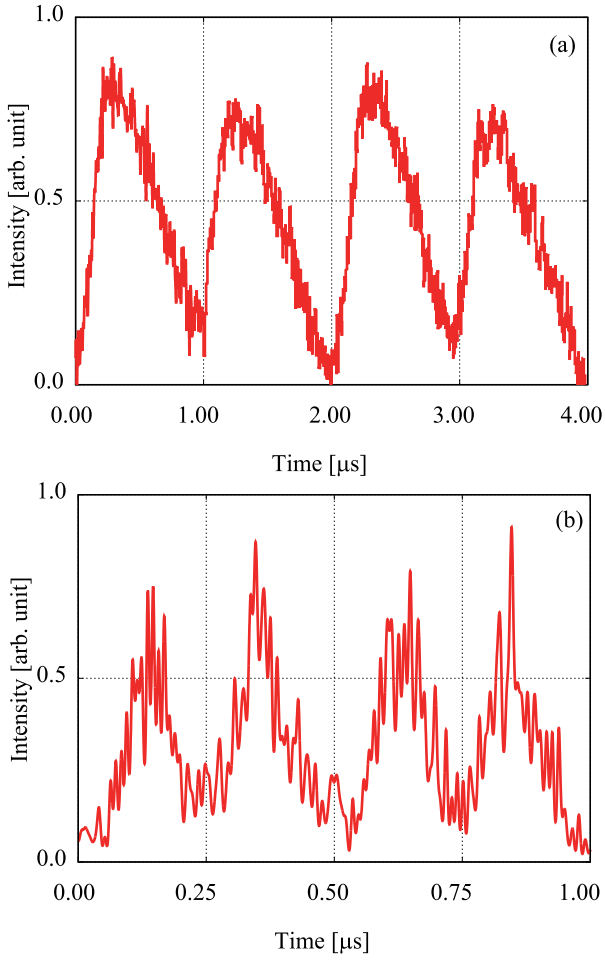

Fig. 4. Variation of light intensity in $\theta = 0$ direction at the siusoidal voltage of (a) 500 kHz and (b) 2 MHz.

channels 5 to 8 differ in phase by π, and the phase difference between adjacent channels changes continuously between 0 and π.

The results of an optical-beam-scanning experiment when frequencies of the sine waves were 500 kHz and 2 MHz are shown in Figs. 4(a) and (b), respectively. The results in Fig. 4(a) indicate that the EO-polymer OPA works at scanning frequency of 500 kHz because the optical beam crosses the 0-degree direction twice in one period (2 μs). The total power consumption of the eight phase shifters under this condition was 0.38 mW; in other words, the EO-polymer OPA has an excellent power-saving performance due to the voltage-control phase shifter. Similarly, the results in Fig. 4(b) indicate that the EO-polymer OPA works even at a high scanning frequency of 2 MHz.

5. Conclusion

A method of driving an EO-polymer OPA with organic silica for cladding was proposed, and the characteristics of the OPA were experimentally investigated. The OPA demonstrated high-speed optical beam scanning at a frequency of 2 MHz when a stable driving waveform superimposing sinusoidal- and rectangular-wave voltages is applied. In addition, the EO-polymer phase shifter can operate with very low power consumption of 0.38 mW at a scanning speed of 500 kHz.

References

[1] P. F. McManamon *et al.*, "A review of phased array steering for narrow-band electrooptical systems," *Proc. IEEE*, vol. 97, no. 6, pp. 1078–1096, Jun. 2009.
[2] I. M. Soganci *et al.*, "160-Gb/s optical packet switching subsystem with a monolithic optical phased-array switch," *IEEE Photon. Technol. Lett.*, vol. 22, no. 11, pp. 817–819, Jun. 2010.
[3] H. Abediasl and H. Hashemi, "Monolithic optical phased-array transceiver in a standard SOI CMOS process," *Opt. Express*, vol. 23, no. 5, pp. 6509–6519, 2015.
[4] Y. Zheng, H. S. Lee, S. Meyne, A. Y. Petrov, and M. Eich, "Waveguide-based optical phased array," *IEEE Photon. Technol. Lett.*, vol. 25, no. 18, pp. 1826–1828, Sep. 2013.
[5] J. Montoya, A. Sanchez-Rubio, R. Hatch, and H. Payson, "Optical phased-array ladar," *Appl. Opt.*, vol. 53, no. 31, pp. 7551–3555, 2014.
[6] J. Sun, E. Timurdogan, A. Yaacobi, E. S. Hosseini, and M. R. Watts, "Large-scale nanophotonic phased array," *Nature*, vol. 493, pp. 195–199, 2013.
[7] M. R. Kossey, C. Rizk, and A. C. Foster, "End-fire silicon optical phased array with half-wavelength spacing," *APL Photon.*, vol. 3, 2018, Art. no. 011301.
[8] K. V. Acoleyern, W. Bogaerts, and R. Baets, "Two-dimensional dispersive on-chip beam scanner fabricated on silicon-on-insulator," *IEEE Photon. Technol. Lett.*, vol. 23, no. 17, pp. 1270–1271, Sep. 2011.
[9] K. V. Acoleyen, H. Rogier, and R. Baets, "Two-dimensional optical phased array antenna on silicon-on-insulator," *Opt. Express*, vol. 18, no. 13, pp. 13 655–13 660, 2010.
[10] K. V. Acoleyen, W. Bogaerts, J. Jagerska, N. L. Thomas, R. Houdre, and R. Baets, "Off-chip beam steering with a one-dimensional optical phased array on silicon-on-insulator," *Opt. Lett.*, vol. 34, no. 9, pp. 1477–1479, 2009.
[11] J. K. Doylend, M. J. R. Heck, J. T. Bovington, J. D. Peters, L. A. Coldren, and J. E. Bowers, "Two-dimensional free-space beam steering with an doptical phased array on silicon-on-insulator," *Opt. Express*, vol. 19, no. 22, pp. 21 595–21 604, 2011.
[12] C. V. Poulton *et al.*, "Large-scale silicon nitride nanophotonic phased arrays at infrared and visible wavelengths," *Opt. Lett.*, vol. 42, no. 1, pp. 21–24, 2017.
[13] S. H. Kim *et al.*, "Thermo-optic control of the longitudinal radiation angle in a silicon-based optical phased array," *Opt. Lett.*, vol. 44, no. 2, pp. 411–414, 2019.
[14] K. V. Acoleyen, K. Komorowska, W. Bogaerts, and R. Baets, "One-dimensional off-chip beam steering and shaping using optical phased arrays on silicon-on-insulator," *J. Lightw. Technol.*, vol. 29, no. 23, pp. 3500–3505, Dec. 2011.
[15] S. Hamann, A. Ceballos, J. Landry, and O. Solgaard, "High-speed random acces optical scanning using a linear mems phased array," *Opt. Lett.*, vol. 43, no. 21, pp. 5455–5458, 2018.
[16] I. P. Kaminow and W. M. Sharpless, "Perfomance of litao3 and linbo3 light modulators at 4 GHz," *Appl. Opt.*, vol. 6, no. 2, pp. 351–352, 1967.
[17] E. L. Wooten *et al.*, "A review of lithium niobate modulators for fiber-optic communications systems," *IEEE J. Sel. Top. Quantum Electron.*, vol. 6, no. 1, pp. 69–82, Jan./Feb. 2000.
[18] W. R. Huang, J. Montoya, J. E. Kansky, S. M. Redmond, G. W. Turner, and A. Sanchez-Rubio, "High speed, high power one-dimensional beam steering from a 6-element optical phased array," *Opt. Express*, vol. 20, no. 16, pp. 17 311–17 318, 2012.
[19] W. Guo, P. R. A. Binetti, C. Althouse, M. L. Masanovic, L. A. Johansson, and L. A. Coldren, "Two-dimensional optical beam steering with inp-based photonic integrated circuits," *IEEE J. Sel. Top. Quantum Electron.*, vol. 19, no. 4, Jul./Aug. 2013, Art. no. 6100212.
[20] J. C. Hulme *et al.*, "Fully integrated hybrid silicon two dimensional beam scanner," *Opt. Express*, vol. 23, no. 5, pp. 5861–5874, 2015.
[21] F. Aflatouni, B. Abiri, A. Rekhi, and A. Hajimiri, "Nanophotonic projection system," *Opt. Express*, vol. 23, no. 16, pp. 21 012–21 022, 2015.
[22] M. Jarrahi, R. F. W. Pease, D. A. B. Miller, and T. H. Lee, "Optical switching based on high-speed phased array optidcal beam steering," *Appl. Phys. Lett.*, vol. 92, 2008, Art. no. 014106.
[23] W. H. Steier *et al.*, "Polymer electro-optic devices for integrated optics," *Chem. Phys.*, vol. 245, pp. 487–506, 1999.
[24] D. Chen, H. R *et al.*, "Demonstration of 110 ghz electro-optic polymer modulators," *Appl. Phys. Lett.*, vol. 70, no. 25, pp. 3335–3337, 1997.
[25] Y. Enami *et al.*, "Hybrid polymer/sol-gel waveguide modulators with exceptionally large electro-optic coefficients," *Nature Photon.*, vol. 1, pp. 180–185, 2007.
[26] Y. Enami *et al.*, "Low half-wave voltage and high electro-optic effect in hybrid polymer/sol-gel waveguide modulators," *Appl. Phys. Lett.*, vol. 89, 2006, Art. no. 143506.
[27] T. Baehr-Jones *et al.*, "Nonlinear polymer-clad silicon slot waveguide modulator with a half wavelength voltage of 0.25 v," *Appl. Phys. Lett.*, vol. 92, 2008, Art. no. 163303.
[28] K. Yamamoto, *et al.*, "Electro-optic waveguide with conductive chromophore contained polymer cladding," *Proc. SPIE*, vol. 8622, 2010, Art. no. 86221K.
[29] Y. Hirano *et al.*, "Demonstration of an optical phased array using electro-optic polymer phase shifters," *Japanese J. Appl. Phys.*, vol. 57, 2018, Art. no. 03EH09.
[30] A. Otomo, I. Aoki, H. Miki, R. Ueda, S. Inoue, and T. Yamada, "Development of sophisticated eo polymer and fabrication of eo modulators," *IEICE Tech. Rep.*, vol. 113, no. 178, pp. 281–285, 2014.